Volume 1 | Number 1 | Jan 2013 | Pages 1–100

Journal of
Materials Chemistry B

Materials for biology and medicine
www.rsc.org/materialsB

ROYAL SOCIETY
OF CHEMISTRY

ROYAL SOCIETY
OF CHEMISTRY

www.rsc.org/materialsB

Gold and silver nanoparticle interactions with human proteins: Impact and

implications in biocorona formation

A. Sasidharan[a], J. E. Riviere[a,b], N. A. Monteiro-Riviere[a*],

[a]Nanotechnology Innovation Center of Kansas State,

[b]Institute of Computational Comparative Medicine,

Department of Anatomy and Physiology, College of Veterinary Medicine,

Kansas State University, Manhattan, Kansas, United States

* Corresponding author. Tel: +1-785-532-4367; fax: +1-785-532-4953.

E-mail address: nmonteiro@ksu.edu

Abstract

The role of nanoparticle (NP) interaction with biomolecules to form a biomolecular corona is the key to NP behavior and its consequences in the physiological environment. Since the adsorbed biocorona decides the fate of a nanomaterial *in vivo,* and thus its successful application in the biomedical arena, a comprehensive understanding of the dynamic interactions of the proteins with the NP is imperative. A systematic investigation on time dependent adsorption kinetics and individual protein corona formation was conducted with citrate and lipoic acid coated 40 nm sized gold (AuNP) and silver NP (AgNP). Both NP were exposed to three major human hard corona proteins; human serum albumin (HSA) (40 mg/ml), fibrinogen (2 mg/ml) and immunoglobulin (IgG) (12 mg/ml) at their physiological concentrations for 24 h. Time evolution data over 0, 6, 12 and 24 h revealed that irrespective of surface chemistry, rapid and prominent binding of HSA and IgG formed coronas over both citrate and lipoic acid coated Au and Ag NP causing an increase in size, without agglomeration up to 24 h at 37°C. In contrast, fibrinogen triggered agglomeration instantaneously upon contact with NP. These findings suggest that irrespective of NP surface chemistry or chemical composition, corona proteins at their physiological concentrations interact rather differently; wherein HSA and IgG coronas adsorbed strongly on the NP surface and kept both Au and AgNP well dispersed, while fibrinogen caused rapid, strong and irreversible agglomeration. Remarkably, individual protein coronas were observed to confer varied cellular uptake patterns for NP-protein complexes in human endothelial cells wherein HSA and IgG coronas showed higher cellular uptake compared to fibrinogen corona.

1. Introduction

Increasing evidence have established that upon exposure to a physiological environment, the NP surface which exhibits high surface energy compared to bulk materials, progressively and selectively adsorbs proteins and other biomacromolecules forming a robust layer described as the "biocorona" .[1-3] The NP-protein corona is a dynamic biological entity, wherein most abundant proteins with high affinity readily adsorb on to the NP surface forming a 'hard corona', over which a rapidly exchanging, loosely associated layer of proteins with a low affinity forms a 'soft corona'. [4, 5] Hard corona proteins have a long-term stability in a biological environment, that can alter the NP synthetic identity like size, shape, surface charge and agglomeration state; as well as its biological identity influencing their cellular internalization, trafficking, opsonization and eventually pattern of biodistribution.[6-10] Recently, Salvati et al.[11] demonstrated that the protein corona can obscure targeting moieties on the NP surface thereby, critically affecting the targeting specificity to cell receptors. All of the above strongly suggests that the biocorona forms the nanobio interface that determines the ultimate biological fate of the NP *in vivo*.

In the past decade, inorganic metal NP are used in biomedical applications owing to their excellent size tunability and unique physicochemical properties. For instance, AgNP have antibacterial and antifungal activity and has been successfully incorporated into wound dressings, medical devices and textiles.[12-16] Similarly, AuNP with brilliant optical properties showcase promising platforms for biosensing, imaging and cancer theranostics.[17-22] However, hurdles

still exist for *in vivo* development for preclinical settings, including biocompatibility, pharmacokinetics, acute and chronic immune responses and toxicity; that depend on its biological identity which is determined by the biocorona. Recently, we have reported that physiological levels of human serum albumin, IgG and transferrin form protein-complexed NP and this protein corona/ NP complex can alter cellular uptake.[7]

Despite such progress, there is a lack of knowledge on how these biological changes and the NP physicochemical properties affect protein binding and corona formation. An improved understanding on the dynamic interaction of the NP-protein and the biocorona formation is needed so that nanomaterials can be designed appropriately for biomedical applications. In this study, we comprehensively analyzed the role of the chemical composition and surface chemistry of the protein-NP interaction using 40 nm citrate and lipoic coated Au and AgNP. Previous studies have recognized human serum albumin (HSA), immunoglobulin (IgG) and fibrinogen to be the major hard corona proteins found to bind firmly on to the NP surfaces and show distinctive stability.[23] Hence, we selected these three long living hard corona proteins and showed that protein-NP interaction and subsequent biocorona formation critically affects the NP dispersion and stability in a time-dependent manner. Moreover, in order to further corroborate the biological outcome of this finding, the cellular uptake of individual NP-protein corona complexes was studied in human primary endothelial cells (HUVEC).

2. Experimental

2.1 Materials

Biopure^{TM} 40 nm citrate and lipoic acid coated Ag and Au NPs (1.00 mg/ml) were obtained from nanoComposix (San Diego, CA). Human serum albumin (HSA), immunoglobulin (IgG) and fibrinogen were purchased from Sigma, (Sigma-Aldrich, MO), HUVEC were procured from Lonza (Lonza, Walkersville, MD) and cultured in EGM-2 medium. Cells were incubated in a humidified atmosphere of 5% CO_2 at 37°C.

2.2 Synthesis of nanomaterials

The 40 nm Au-NPs (1.0mg/ml) and Ag-NPs (1.0mg/ml) were obtained from nanoComposix (San Diego, CA). AuNP were synthesized via the reduction of tetrachloroauric acid onto 7 nm Au seed particles in a sodium citrate buffer. Ag NP were synthesized by ammonium hydroxide catalyzed growth of ionic silver onto 20 nm Ag seed particles in a sodium citrate buffer. The Au and Ag metal purity of the respective particles is >99.99% as measured with inductively coupled plasma mass spectrometry (ICP-MS). NP were concentrated via tangential flow filtration, serially washed and suspended in deionized water. The manufacturer characterized each batch with transmission electron microscopy (TEM) to determine size and shape distributions, UV-visible spectroscopy to measure the optical properties, particle hydrodynamic diameter with dynamic light scattering, and particle surface charge with a zeta potential measurement. Mass concentration was determined with ICP-MS. The NPs were

sterile filtered and tested for endotoxin before delivery. Upon arrival, the AgNPs

were stored at 4°C in the dark.

2.3 Physicochemical characterization of nanomaterials

Transmission electron microscopy (TEM) was used to measure the average

diameter and morphology of the both Au and AgNP. For high resolution TEM,

5µl of each NP suspensions were drop onto carbon coated grids. Samples were

visualized with the Tecnai G2 Spirit BioTWIN with an acceleration voltage of 120

kV.   Dynamic light scattering (DLS) and zeta-potential analysis (Malvern

Zetasizer Nano ZS, UK) was performed to study the size distribution and surface

charge at a concentration of 50 µg/ml at 25°C.

2.4 Protein binding study

Citrate and lipoic acid coated 40 nm Au and AgNP was added to proteins

solutions at their respective physiological concentration; 40 mg/ml HSA, 12mg/ml

IgG, and 2mg/ml fibrinogen in phosphate buffered saline (PBS).   These NP-

protein complexes were then incubated at 37°C for 0, 6, 12 and 24 h.

2.5 TEM imaging of protein corona

The individual protein corona formation was visualized via TEM. After 6 h of

incubation with a representative protein and NP, HSA and Au, respectively, the

NP-protein complexes were repeatedly washed with phosphate buffered saline

(PBS) and the supernatant was removed.   The NP-protein complex pellet was

resuspended and fixed using 2.5% glutaraldehyde for 1 h. For TEM imaging, 5 µl

of the NP protein complex was placed onto the carbon coated copper grids and imaged with the Tecnai G2 Spirit BioTWIN TEM with an acceleration voltage of 120 kV.

2.6 Cellular uptake studies of NP-protein complex

HUVEC were grown on 13mm glass cover slips placed within 12-well plate at seeding density of 3000 cells/cover slip. After 24 h, NP-protein complexes were incubated with cells for 24 h and the cellular uptake was analyzed using the CytoViva® hyperspectral imaging system (CytoViva, Inc., Auburn, AL) equipped with an Olympus BX53 dark field microscope. Spectral characterization was further analyzed using ENVI 4.4 software.

3. Results and Discussion

It is now accepted that NP possessing a high surface-to-volume ratio acts like a scaffold and adsorbs proteins over their entire surface to form a nano-bio interface known as the protein corona, effectively reducing their surface energy.[24, 25] In this study, 40 nm sized citrate and lipoic coated Au and Ag NPs with three major corona protein constituents, HSA, IgG and fibrinogen at their physiological concentrations were investigated and the effect of chemical composition and surface chemistry on the protein-NP interactions and role of the formed biocorona on the dispersion and stability of NPs.

3.1. Physicochemical characterization of NP

Methodical physicochemical characterization of NP with TEM, DLS and zeta potential analyses was performed. As shown in Fig. 1a-d, TEM images conclusively confirmed that the synthesized Au and AgNP were spherical, and highly monodispersed. The average hydrodynamic diameter for citrate-Au was 43.7 nm and lipoic acid-AuNP was 48.4 nm in milli-Q water, while citrate-Ag was 43.1 nm and lipoic-Ag was 48.7 nm (Fig.1 a1-d1). Table 1 summarizes the physicochemical characterization data of the NPs. Surface charge analysis revealed that all tested Au and AgNPs had a net negative charge. Citrate-Au and lipoic-Au exhibited -50.5 mV and -46.6 mV, whereas citrate-Ag and lipoic-Ag revealed slightly lower values of -41.5 and -44.6, respectively. Collectively, physicochemical characterization of citrate and lipoic coated Au and AgNP revealed a highly monodispersed, homogenous, 40nm sized NP exhibiting a net negative charge with excellent stability.

3.2 NP-protein interaction and individual corona formation

In order to investigate the protein binding dynamics and individual protein corona formation, time dependent changes in size distribution and surface charge of the individual Au and AgNP (n=4) and proteins (n=3) dispersed in 10 % phosphate buffered saline (PBS) at 37°C for 24 h was monitored. As shown in Fig. 2a-d the size distribution analysis showed a slight increase in the hydrodynamic diameter of citrate and lipoic coated Au and AgNP incubated in PBS, compared to NP dispersed in water only. Importantly, NP suspensions remained stable over a 0,

6, 12 and 24 h. However, the proteins showed a broad size distribution ranging from 10-400 nm (Fig. 2 e-g). HSA displayed an even, bimodal size distribution pattern with a sharp primary peak in the range of 0-10 nm and a secondary, broader peak in the range of 10-300 nm, throughout 24 h. IgG showed a wide, multivariate size distribution pattern indicating time dependent changes in size. In contrast, fibrinogen exhibited significant changes from the initial size after 6 h. In addition to the primary peak in the range of 0-50 nm, a wide, high intensity secondary peak in the range of 250-400 nm was noted. At 24 h, fibrinogen showed a primary peak with a shoulder in the range of 45-80 nm and secondary peak shift to the range of 200-400 nm.

In order to further investigate variations in surface charge, zeta potential was used to monitor the possible variations in the net surface charge of the NP protein exposure as well as to gain an insight into the nanomaterial dispersion or agglomeration status. NP in PBS showed a marked reduction in the surface charge compared to the NP in milli-Q water (Table S1, Supplementary Information). Citrate-Au exhibited a slow decrease in surface charge in the range of -11.2 to -10.9 and lipoic-Au showed a significant decrease from -19.8 to -12.4 over 24h. Whereas, citrate-Ag showed a relatively higher zeta potential of -25.9 to -17.3 and lipoic-Ag showed -33.4 to -20.1 under similar conditions. Zeta potential analysis of HSA, IgG and fibrinogen are shown in Table S2, Supplementary Information. Both HSA and fibrinogen exhibited a net negative charge ranging from -12.8 to -11.8 mV for HSA and -5.51 to -4.86 mV for

fibrinogen. IgG displayed a positive surface charge in the range of 5.50 to 4.99.
Interestingly, recent studies have also documented that these three proteins
show high binding affinity to the NP surface to form a distinctively stable, hard
corona.[8, 25]

3.2.1 NP-HSA interaction

HSA (MW: 66 kDa) is the major constituent serum protein found in adult human
plasma, which aids in transporting hormones, fatty acids, and a host of other
compounds, and maintains osmotic pressure, among other functions.[26] The
reference range for HSA concentrations in serum is approximately 40 mg/ml.
Time dependent individual HSA corona formation was monitored by changes in
NP size and surface charge at defined time periods of 0, 6, 12 and 24 h at 37°C.
Fig. 3a1-a4 demonstrates that Au-HSA and Ag-HSA corona formation exhibited a
bimodal size distribution similar to that of the HSA solution, but with higher
intensities, masking the characteristic NP size distribution pattern. Citrate Au-
HSA corona showed a reduced intensity primary peak in 0-10 nm size range and
a high intensity secondary peak appearing in 50-400 nm range. Lipoic-Au-HSA
corona showed a comparatively higher intensity primary peak and a lower
intensity secondary peak. Citrate Ag-HSA and lipoic Ag-HSA showed similar
adsorption patterns with slight differences in intensity and peak shift of the
secondary peak. These results suggest that HSA established a stronger
interaction with lipoic acid coated Au and Ag NP than with citrate coated NPs.
Potentially, lipoic acid coating being more stable than citrate coating could have

aided the HSA to bind strongly to lipoic Au and Ag NP, which suggests the important role of the NP surface chemistry in protein adsorption. However, unlike surface chemistry, our results show no apparent role for core chemical composition in protein binding. The most striking observation is that all NP-HSA coronas exhibited a similar size distribution patterns, mirroring the HSA size distribution. Zeta potential measurements of Au and AgNP-HSA coronas are shown in Table 2. As expected, all NP-HSA coronas exhibited a negative surface charge in the range of -7.91 to -12.7 mV. There were no major variations in zeta potential over 24 h.

3.2.2 NP-IgG interaction

Representing ~75% of serum immunoglobulins in humans, IgG (MW: 150 kDa) is the most abundant antibody isotype found in the circulation that plays an important role in the immune defense mechanisms.[27] IgG concentration in human blood plasma is ~12 mg/ml. Fig. 3b1-b4 shows the size distribution of Au-IgG and Ag-IgG coronas, which revealed identical size distribution peaks, which were stable over a period of 24 h except for citrate Au-IgG which showed peak shifts over a range of 240-300 nm. Regardless of the bare NP size distribution pattern, similar to NP-HSA corona, NP-IgG corona also showed a bimodal size distribution pattern suggesting rapid binding of IgG onto the NP surface. Table 3 summarizes the surface charge of NP-IgG coronas. Interestingly, the net negative surface charge of NPs was shifted to the positive scale with higher zeta potential values for lipoic-NP-IgG coronas over citrate-NP-IgG coronas indicating

higher stability of the lipoic-NP-IgG coronas (Table 3). The lipoic coated NP exhibited high stability compared to citrate coated NP, which might be the possible reason for the higher binding affinity of IgG towards the citrate surface.

3.2.3 NP-Fibrinogen interaction

Fibrinogen (MW: 340 kDa) is the largest protein with a unique molecular dimension (6 x 6 x 45 nm) responsible for regulating hemostasis and the inflammatory response and is present in blood plasma at a concentration of 2-4 mg/ml.[28] Subsequently, the interaction of fibrinogen with all of the tested NP were studied for 24 h. Remarkably, despite a low concentration of 2 mg/ml, fibrinogen triggered rapid and severe agglomeration upon exposure with the NP suspension. The size distribution pattern in Fig. 3c1-c4 depicts that irrespective of the difference in surface chemistry, material composition or incubation time, fibrinogen corona induced agglomeration in Au and Ag NPs. Zeta potential analysis results indicated adsorption of fibrinogen onto the NP surface leading to a reduction in surface charge with all NPs, which showed a similar trend over 24 h (Table S3, Supplementary Information).

The most striking observation noted, irrespective of surface chemistry or chemical composition, was that fibrinogen triggered a rapid and irreversible agglomeration with Au and AgNP. It has long been postulated that the adsorption of proteins on to NP surfaces increases the colloidal stability and the observed fibrinogen induced an aggregation of NP which challenges the broad application

of this hypothesis.[29] Previous studies have demonstrated that the formation of a biocorona also depends on the protein concentration, their association and dissociation rate.[1, 3, 30, 31]   Interestingly, our results showed that at low concentrations of fibrinogen (2mg/ml) agglomeration was triggered to form small and large NP aggregates. However, similar observations where fibrinogen induced agglomeration of carbon nanotubes have been reported.[32] It can be speculated that the observed aggregation could be due to the elongated rod like conformation and unique molecular dimension of fibrinogen. [33]

3.2.4 Protein corona formation in a competitive environment

In an attempt to learn whether HSA or IgG could reverse or inhibit agglomeration induced by fibrinogen, NPs were incubated in HSA-fibrinogen and HSA-IgG-fibrinogen mixture, at their respective physiological concentrations, for 24h to mimic a competitive environment. From Fig. 4a1-a4 it could be seen that fibrinogen induced agglomeration of NP, evident from the peak shift of the X-axis well into micrometer range. As shown in Table S4 (Supplementary Information), all tested NP displayed a lower zeta potential, which confirmed lower stability leading to agglomeration. To study the agglomeration status in the presence of IgG along with HSA and fibrinogen, NPs were also incubated with a HSA-IgG-fibrinogen mixture. However, fibrinogen was shown to trigger agglomeration even with the presence of HSA and IgG as seen in Fig 4b1-b4. Tested NPs registered low zeta potential values associated with low stability (Supplementary Information; Table S5). To rule out any chances of agglomeration or unusual

dynamics of NPs in a HSA-IgG protein system, NPs were also incubated in a HSA-IgG mixture. In contrast to individual HSA and IgG coronas, the HSA-IgG mixture showed a reduced intensity primary peak in 0-10 nm size range. The zeta potential analysis in Table S6 (Supplementary Information) exhibited a negative surface charge for all the tested combinations. These results show that despite the presence of a relatively higher concentration of HSA (40 mg/ml) or IgG (12 mg/ml), fibrinogen triggered agglomeration. It could be assumed that the rigid fibrinogen molecules competed with the conformationally flexible HSA, to adsorb onto the NP and induce aggregation. Within the stipulated time, considering the relative abundance of HSA or IgG, fibrinogen was not replaced by HSA or IgG to reverse aggregation, indicative from the presence of NP aggregates at 24 h. This phenomenon could have profound biological implications for NP biodistribution where upon entry in to interstitial spaces rich in fibrinogen, NPs could agglomerate and get trapped.

3.3 Visualization of the protein corona

In order to obtain direct evidence on individual protein corona formation on the NP surface, morphological analysis was done using TEM (Fig. 5a-b1). TEM imaging of adsorbed protein corona requires sample fixation and processing, and hence, we have selected stable AuNP as a representative NP over AgNP, which exhibits possible artifacts from its dissolution properties.[7] TEM analysis revealed an even, thin shell of HSA corona formed over the citrate and lipoic coated AuNP (Fig. 5a1-b1). Presence of the corona encompassing the AuNP even after

14

multiple washing steps is indicative of a stable, strong and persistent adsorption of HSA hard corona over NP surface.

3.4 Cellular uptake of nanoparticle-protein complex in HUVECs

The observed changes in the individual protein adsorption and protein corona formation may have implications in the biological fate of NP. We and others have shown that the difference in the protein corona composition influences the cellular uptake of NP.[7, 11] Nevertheless, NPs are generally introduced into the human body through systemic administration thereby, resulting in direct exposure to the endothelial cells.[34] Therefore, it is imperative to investigate the cellular uptake of NP in endothelial cells. Fig. 6a-d depicts the intracellular distribution of a representative NP-protein corona in HUVEC as determined by hyperspectral microscopy. Untreated cells served as the control (Fig. 6a). Interestingly, citrate-Au-HSA and citrate-Au-IgG coronas exhibited high cellular uptake compared to citrate-Au-fibrinogen corona, which showed markedly reduced uptake, possibly due to NP agglomeration. The corresponding hyperspectral plots (Fig. 6 b, c and d insets) confirmed the presence of AuNP within the cells. Here, the nature of the biocorona played a critical role in the particle stability thereby influencing cellular uptake in HUVEC. One may speculate that the observed difference in the individual protein binding can influence the *in vivo* biodistribution pattern as well.[30, 35] For instance, NP-HSA corona or NP-IgG corona may prolong blood circulation times, while NP-fibrinogen corona may cause rapid accumulation within organs. The sensitivity of NP protein corona composition to proteins

present, as demonstrated in our study, also has implications to extrapolating NP biodistribution across species since differences in plasma protein composition will effect NP corona composition and hence, patterns of *in vivo* biodistribution. In addition to actual composition, kinetic differences in corona formation could also impact biodistribution when doing *in vitr*o to *in vivo* extrapolations or when predicting human distribution from observations from rodent data with shorter blood circulation times.[35] We recognize that our studies looked at NP interactions of only three proteins when *in vivo*, hundreds of proteins are involved in NP corona formations.[4, 36, 37] However, this simple model system across four NP systems and three relevant and important corona proteins demonstrates some fundamental principles that must be considered when more complex systems are studied, for example how fibrinogen and albumin interactions dictate corona properties.

5. Conclusion

In summary, these results demonstrate that the nature of individual proteins play a significant role in the protein binding and subsequent corona formation over the Au and AgNP surfaces. Irrespective of NP composition or surface chemistry, HSA and IgG showed a strong prominent binding on both Au and AgNP. Surprisingly, fibrinogen at a relatively low physiological concentration induced rapid, severe, and irreversible agglomeration. In addition, our cellular uptake profiles corroborated the formation of individual protein coronas which

16

showcased distinct intracellular uptake patterns. Collectively, our data suggests that the nature of the biointeraction of each individual protein is very different, thereby potentially affecting the biological response of NPs. These findings may shed light towards the necessity of appropriate designing of nanomaterials for future successful *in vivo* biomedical applications.

Acknowledgements

References

1. T. Cedervall, I. Lynch, S. Lindman, T. Berggård, E. Thulin, H. Nilsson, K. A. Dawson and S. Linse, *Proceedings of the National Academy of Sciences of the United States of America*, 2007, 104, 2050-2055.
2. M. Lundqvist, J. Stigler, G. Elia, I. Lynch, T. Cedervall and K. Dawson, *Proceedings of the National Academy of Sciences*, 2008, 105, 14265-14265.
3. F. Darabi Sahneh, C. Scoglio and J. Riviere, *PloS one*, 2013, 8, e64690-e64690.
4. M. P. Monopoli, D. Walczyk, A. Campbell, G. Elia, I. Lynch, F. B. Bombelli and K. A. Dawson, *Journal of the American Chemical Society*, 2011, 133, 2525-2534.
5. E. Casals, T. Pfaller, A. Duschl, G. J. Oostingh and V. Puntes, *ACS nano*, 2010, 4, 3623-3632.
6. S. Tenzer, D. Docter, J. Kuharev, A. Musyanovych, V. Fetz, R. Hecht, F. Schlenk, D. Fischer, K. Kiouptsi, C. Reinhardt, K. Landfester, H. Schild, M. Maskos, S. K. Knauer and R. H. Stauber, *Nature nanotechnology*, 2013, 8, 772-781.
7. N. A. Monteiro-Riviere, M. E. Samberg, S. J. Oldenburg and J. E. Riviere, *Toxicology letters*, 2013, 220, 286-293.
8. C. D. Walkey and W. C. W. Chan, *Chemical Society reviews*, 2012, 41, 2780-2799.
9. J. E. Riviere, *Wiley interdisciplinary reviews. Nanomedicine and nanobiotechnology*, 1, 26-34.
10. C. Y. Tay, M. I. Setyawati, J. Xie, W. J. Parak and D. T. Leong, *Advanced Functional Materials*, 2014, 24, 5936-5955.
11. A. Salvati, A. S. Pitek, M. P. Monopoli, K. Prapainop, F. B. Bombelli, D. R. Hristov, P. M. Kelly, C. Åberg, E. Mahon and K. A. Dawson, *Nature nanotechnology*, 2013, 8, 137-143.
12. N. A. Monteiro-Riviere and C. L. Tran, *informa healthcare*.
13. K. Chaloupka, Y. Malam and A. M. Seifalian, *Trends in biotechnology*, 2010, 28, 580-588.
14. M. E. Samberg, P. E. Orndorff and N. A. Monteiro-Riviere, *Nanotoxicology*, 2011, 5, 244-253.
15. M. E. Samberg, Z. Tan, N. A. Monteiro-Riviere, P. E. Orndorff and R. A. Shirwaiker, *Journal of materials science. Materials in medicine*, 2013, 24, 755-760.
16. M. E. Samberg, P. Mente, T. He, M. W. King and N. A. Monteiro-Riviere, *Annals of biomedical engineering*, 2014, 42, 1482-1493.
17. E. C. Dreaden, A. M. Alkilany, X. Huang, C. J. Murphy and M. A. El-Sayed, *Chemical Society reviews*, 2012, 41, 2740-2779.
18. L. Dykman and N. Khlebtsov, *Chemical Society reviews*, 2012, 41, 2256-2282.
19. F. Jia, X. Liu, L. Li, S. Mallapragada, B. Narasimhan and Q. Wang, *J Control Release*, 2013, 172, 1020-1034.
20. M. S. Bhojani, M. Van Dort, A. Rehemtulla and B. D. Ross, *Mol Pharm*, 2010, 7, 1921-1929.
21. S. M. Janib, A. S. Moses and J. A. MacKay, *Adv Drug Deliv Rev*, 2010, 62, 1052-1063.

22.   D. T. Leong and K. W. Ng, *Adv Drug Deliv Rev*, 2014, 79-80c, 95-106.
23.   M. Mahmoudi, I. Lynch, M. R. Ejtehadi, M. P. Monopoli, F. B. Bombelli and S. Laurent, *Chemical reviews*, 2011, 111, 5610-5637.
24.   I. Lynch and K. A. Dawson, *Nano Today*, 2008, 3, 40-47.
25.   M. Mahmoudi, K. Azadmanesh, M. Shokrgozar, W. Journeay and S. Laurent, *Chemical reviews*, 2011.
26.   personal communication.
27.   H. W. Schroeder and L. Cavacini, *The Journal of allergy and clinical immunology*, 2010, 125, S41-52.
28.   M. W. Mosesson, *Journal of thrombosis and haemostasis : JTH*, 2005, 3, 1894-1904.
29.   A. E. Nel, L. Mädler, D. Velegol, T. Xia, E. M. V. Hoek, P. Somasundaran, F. Klaessig, V. Castranova and M. Thompson, *Nature materials*, 2009, 8, 543-557.
30.   F. D. Sahneh, C. M. Scoglio, N. A. Monteiro-Riviere and J. E. Riviere, *Nanomedicine (London, England)*, 2014, DOI: 10.2217/nnm.14.60, 1-9.
31.   G. Caracciolo, D. Pozzi, A. L. Capriotti, C. Cavaliere, P. Foglia, H. Amenitsch and A. Lagana, *Langmuir*, 2011, 27, 15048-15053.
32.   S. H. De Paoli, L. L. Diduch, T. Z. Tegegn, M. Orecna, M. B. Strader, E. Karnaukhova, J. E. Bonevich, K. Holada and J. Simak, *Biomaterials*, 2014, 35, 6182-6194.
33.   B. Lassen and M. Malmsten, *Journal of Colloid and Interface Science*, 1996, 180, 339-349.
34.   A. Sasidharan, P. Chandran, D. Menon, S. Raman, S. Nair and M. Koyakutty, *Nanoscale*, 2011, 3, 3657-3669.
35.   J. E. Riviere, *Nanomedicine (London, England)*, 2013, 8, 1357-1359.
36.   M. P. Monopoli, C. Aberg, A. Salvati and K. A. Dawson, *Nature nanotechnology*, 2012, 7, 779-786.
37.   D. Walczyk, F. B. Bombelli, M. P. Monopoli, I. Lynch and K. A. Dawson, *Journal of the American Chemical Society*, 2010, 132, 5761-5768.

Graphical Abstract

Metallic NP interaction with human proteins, biocorona formation and their impact on cellular uptake.

Figures Legends

Fig. 1. TEM images of (a) citrate-Au, (b) lipoic-Au, (c) citrate-Ag and (d) lipoic-Ag. DLS analysis of (a1) citrate-Au, (b1) lipoic-Au, (c1) citrate-Ag and (d1) lipoic-Ag.

Fig. 2. Time dependent size distribution analysis of test nanoparticles: (a) citrate-Au, (b) lipoic-Au, (c) citrate-Ag and (d) lipoic-Ag, and test proteins: (e) HSA, (f) IgG and (g) fibrinogen.

Fig. 3. Time dependent size distribution profiling of HSA corona over (a1) citrate-Au, (a2) lipoic-Au, (a3) citrate-Ag and (a4) lipoic-Ag, IgG corona over (b1) citrate-Au, (b2) lipoic-Au, (b3) citrate-Ag and (b5) lipoic-Ag and fibrinogen corona over (c1) citrate-Au, (c2) lipoic-Au, (c3) citrate-Ag and (c4) lipoic-Ag.

Fig. 4. Time dependent size distribution profiling of HSA + fibrinogen corona over (a1) citrate-Au, (a2) lipoic-Au, (a3) citrate-Ag and (a4) lipoic-Ag and HSA +IgG +

fibrinogen corona over (b1) citrate-Au, (b2) lipoic-Au, (b3) citrate-Ag and (b4) lipoic-Ag.

Fig. 5. TEM images of (a) bare citrate-Au NP and (a1) citrate-Au-HSA corona and (b) bare lipoic-Au NP and (b1) lipoic-Au-HSA corona .

Fig. 6. Representative dark-field images of NP-protein complex treated with HUVEC: (a) Control, (b) citrate-Au-HSA, (c) citrate-Au-IgG and (d) citrate-Au-fibrinogen. Inset: Hyperspectral profile measurement. Scale bar: 50µm.

Table 1. Summary of the physicochemical characterization data for citrate and lipoic acid coated Au and Ag NP in milli-Q water.

Table 2. Time dependent zeta potential of analysis of NP-HSA corona.

Table 2. Time dependent zeta potential of analysis of NP-HSA corona.

Table 1. Summary of the physicochemical characterization data for citrate and lipoic acid coated Au and Ag NP in milli-Q water.

NP	Surface coating	TEM (nm)	DLS (nm)	Polydispersity index (PdI)	Zeta potential (mV)
Gold	Citrate	38.1 ± 4.3	43.7 ± 4.2	0.118	-50.5 ± 3.7
	Lipoic	41.3 ± 4.9	48.4 ± 2.4	0.063	-46.6 ± 2.3
Silver	Citrate	41.9 ± 4.8	43.1 ± 3.1	0.145	-41.5 ± 1.8
	Lipoic	40.3 ± 4.6	48.7 ± 2.1	0.117	-44.6 ± 2.5

Table 2. Time dependent zeta potential of analysis of NP-HSA corona.

Time (h)	Citrate-Au-HSA (mV)	Lipoic-Au-HSA (mV)	Citrate-Ag-HSA (mV)	Lipoic-Ag-HSA (mV)
0	-7.91 ± 2.9	-9.77 ± 3.7	-10.8 ± 2.5	-12.7 ± 2.13
6	-8.74 ± 2.3	-9.63 ± 1.1	-11.6 ± 3.3	-12.4 ± 2.14
12	-8.63 ± 1.2	-8.53 ± 2.1	-10.68 ± 3.0	-11.8 ± 3.21
24	-9.04 ± 3.8	-10.68 ± 3.7	-9.6 ± 2.1	-11.6 ± 4.4

Table 3. Time dependent zeta potential analysis of NP-IgG corona.

Time (h)	Citrate-Au-IgG (mV)	Lipoic-Au-IgG (mV)	Citrate-Ag-IgG (mV)	Lipoic-Ag-IgG (mV)
0	0.15 ± 0.2	0.42 ± 0.4	0.34 ± 0.23	0.46 ± 0.5
6	0.24 ± 0.8	0.50 ± 0.13	0.32 ± 0.1	0.52 ± 0.4
12	0.39 ± 0.4	0.58 ± 0.1	0.36 ± 0.24	0.58 ± 0.5
24	0.35 ± 0.13	0.66 ± 0.12	0.42 ± 0.06	0.66 ± 0.3
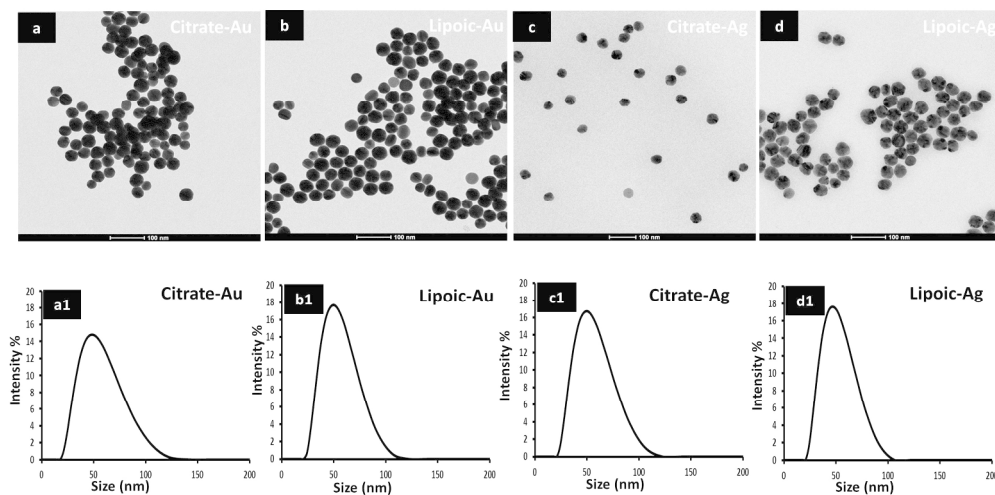
Fig. 1. TEM images of (a) citrate-Au, (b) lipoic-Au, (c) citrate-Ag and (d) lipoic-Ag. DLS analysis of (a1) citrate-Au, (b1) lipoic-Au, (c1) citrate-Ag and (d1) lipoic-Ag.
254x126mm (300 x 300 DPI)
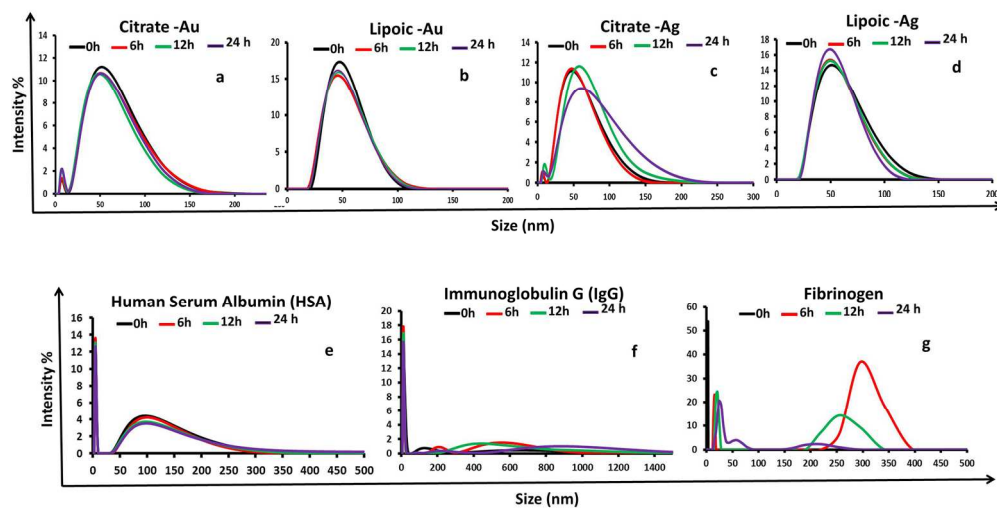
Fig. 2. Time dependent size distribution analysis of test nanoparticles: (a) citrate-Au, (b) lipoic-Au, (c) citrate-Ag and (d) lipoic-Ag, and test proteins: (e) HSA, (f) IgG and (g) fibrinogen.
254x134mm (200 x 200 DPI)
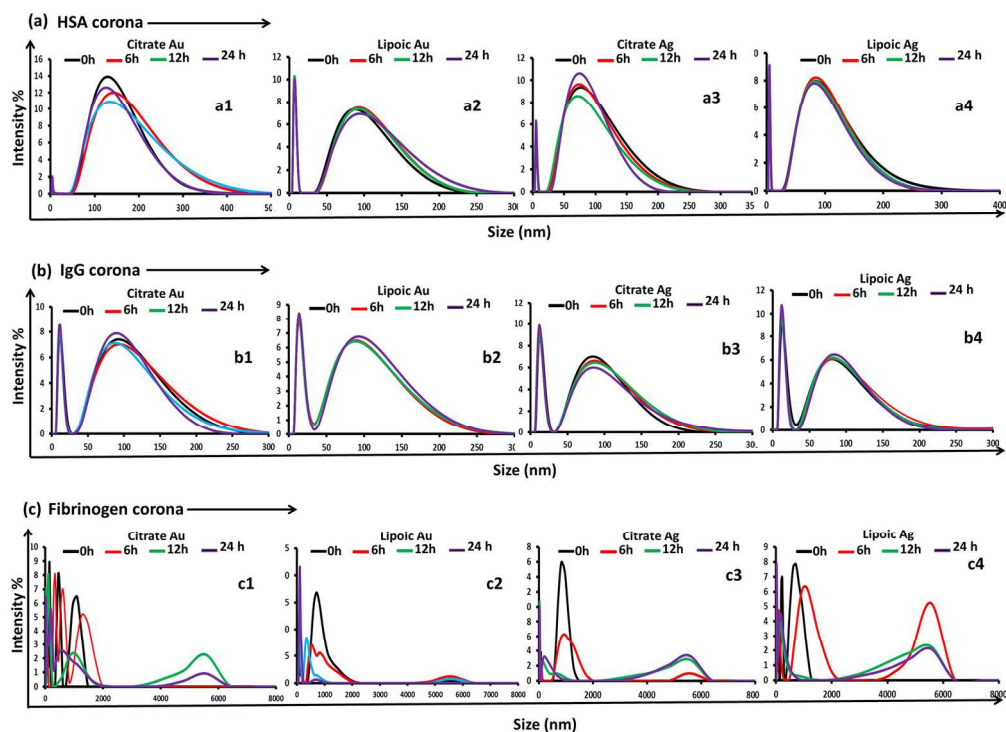
Fig. 3. Time dependent size distribution profiling of HSA corona over (a1) citrate-Au, (a2) lipoic-Au, (a3) citrate-Ag and (a4) lipoic-Ag, IgG corona over (b1) citrate-Au, (b2) lipoic-Au, (b3) citrate-Ag and (b5) lipoic-Ag and fibrinogen corona over (c1) citrate-Au, (c2) lipoic-Au, (c3) citrate-Ag and (c4) lipoic-Ag.
254x190mm (200 x 200 DPI)
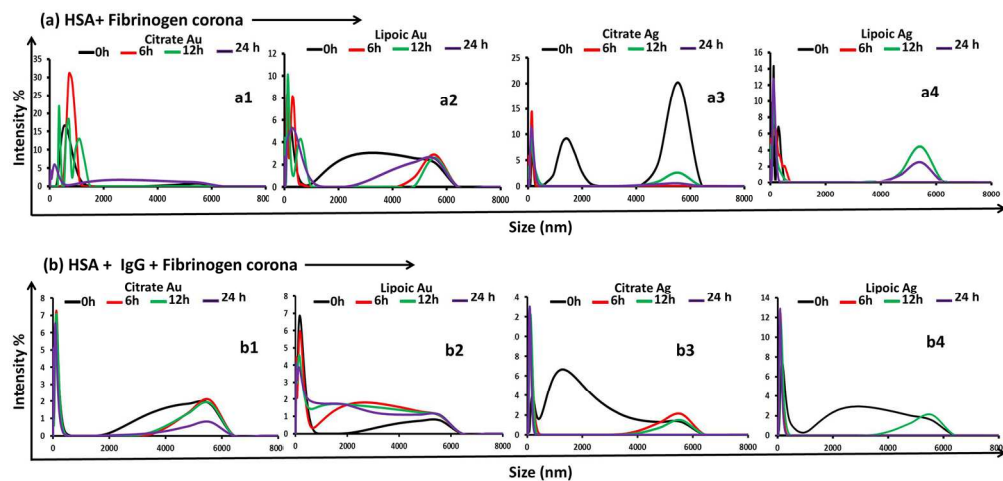
Fig. 4. Time dependent size distribution profiling of HSA + fibrinogen corona over (a1) citrate-Au, (a2) lipoic-Au, (a3) citrate-Ag and (a4) lipoic-Ag and HSA +IgG + fibrinogen corona over (b1) citrate-Au, (b2) lipoic-Au, (b3) citrate-Ag and (b4) lipoic-Ag.
254x124mm (200 x 200 DPI)
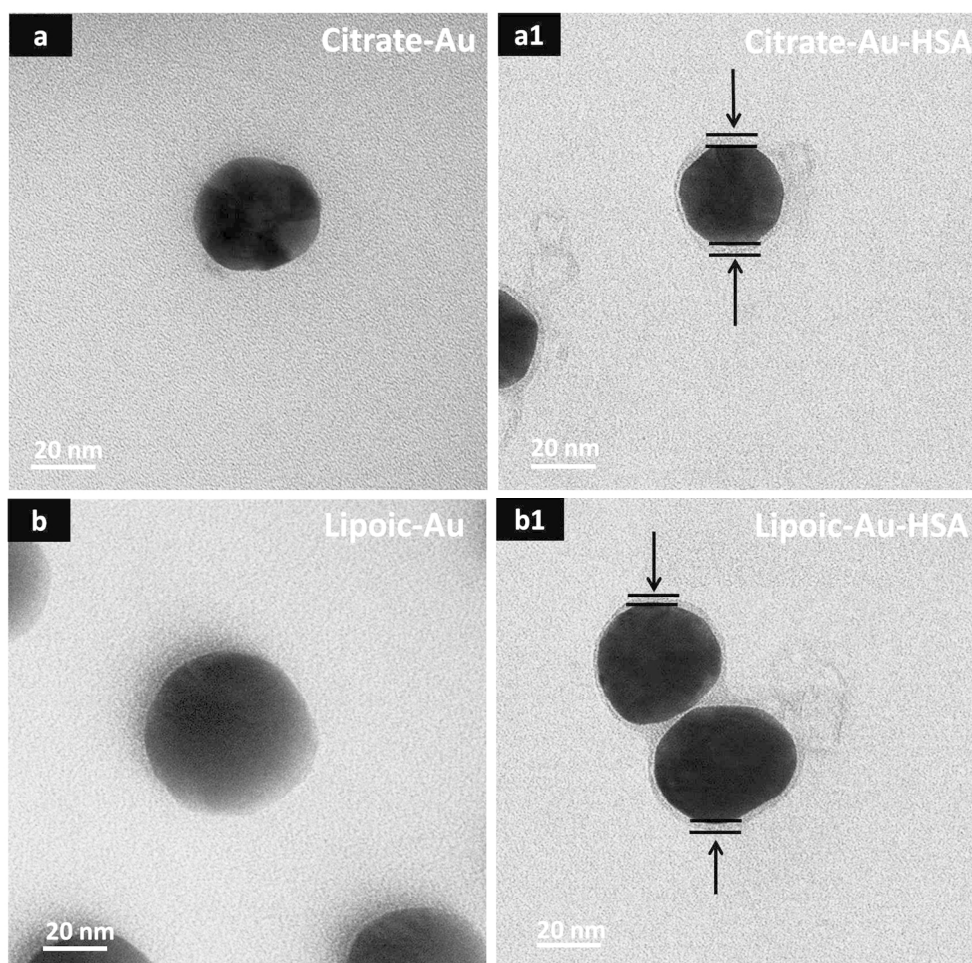
Fig. 5. TEM images of (a) bare citrate-Au NP and (a1) citrate-Au-HSA corona and (b) bare lipoic-Au NP and (b1) lipoic-Au-HSA corona .
154x154mm (300 x 300 DPI)
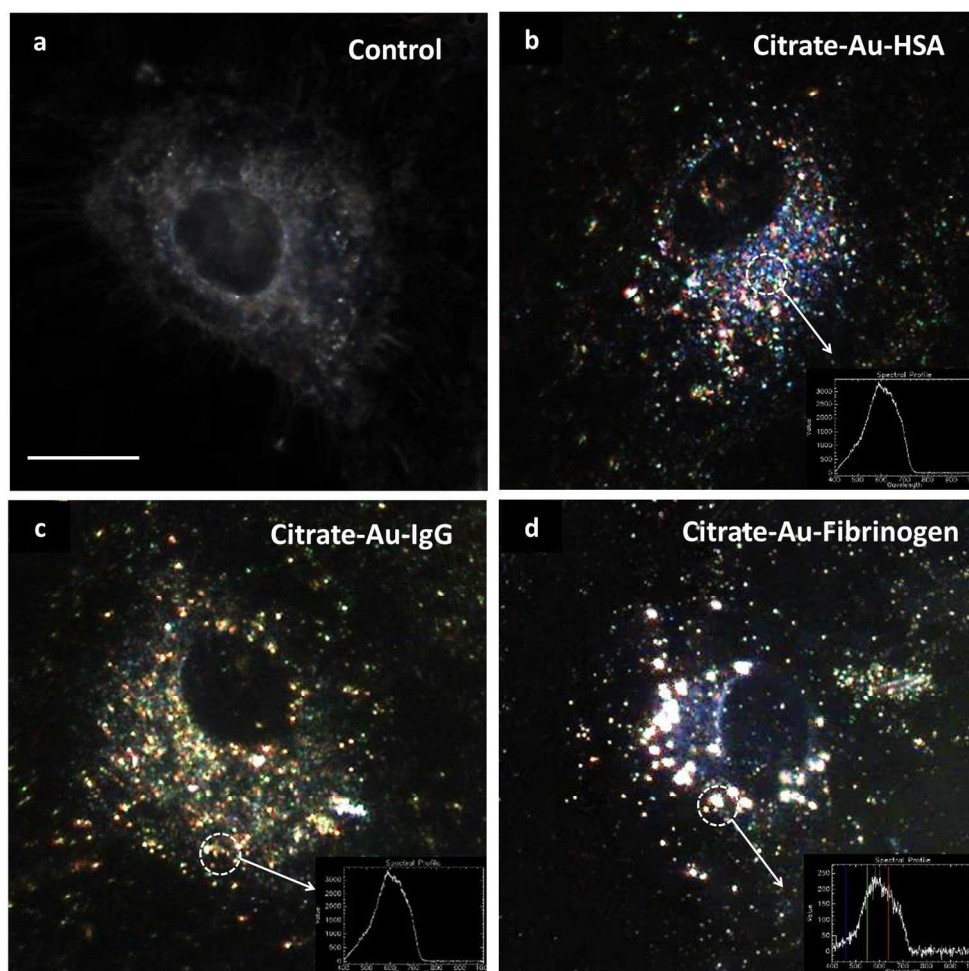
Fig. 6. Representative dark-field images of NP-protein complex treated with HUVEC: (a) Control, (b) citrate-Au-HSA, (c) citrate-Au-IgG and (d) citrate-Au-fibrinogen. Inset: Hyperspectral profile measurement. Scale bar: 50μm.
478x479mm (96 x 96 DPI)
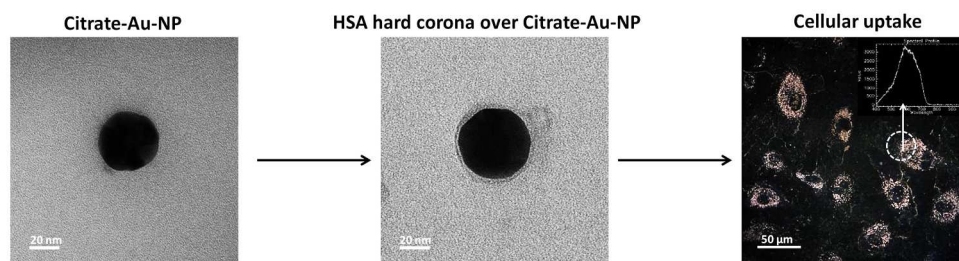
Citrate-Au-NP   **HSA hard corona over Citrate-Au-NP**   **Cellular uptake**

Metallic NP interaction with human proteins, biocorona formation and their impact on cellular uptake.

223x63mm (300 x 300 DPI)